# Serial-arc detection by use of Spectral Dispersion Index (SDI) analysis in a low-voltage network (270V HVDC)

Jean Baptiste Humbert, Patrick Schweitzer, Serge Weber

Version of Record: https://www.sciencedirect.com/science/article/pii/S0378779621000651
Manuscript_06eb3ab40246a7016ddff05f47f2fd38



# Series Arc Fault Location Algorithm Based on Impedance parameters and Fault Map Trace Generation

Jean Baptiste Humbert, Patrick Schweitzer, and Serge Weber
University of Lorraine, CNRS, Institut Jean Lamour (IJL), Nancy F-54000, France

***Abstract*—In this paper we will present a method for detecting series-arc faults, based on a frequency analysis that uses a decision block. We will define the parameters of a Spectral Dispersion Index SDIthat has been calculated using data taken from a binarized spectrogram of the line current (provided by employing a dynamic-thresholding process). The decision block 'uses a counter mechanism that increased or decreased in value at a quicker or slower rate, depending on whether or not a fault was present in the power line. The status of its operating mode was recorded using a finite-state machine. In this method of detection, a trip indicator is activated whenever a fault is present. The method was tested on a large variety of loads, including resistive, inductive and switching loads. The confusion matrix we obtained, showed that series-arc faults can be successfully detected in this way. We will therefore be able to minimize the number of false detections that often occur in the case of switching loads or voltage generators.**

***Index Terms*—Series arc fault, arcing fault detection, DC power network, frequency analysis.**

## I. Introduction

The use of DC power grids has expanded widely during recent years. In the aeronautics sector, voltage-supply levels are tending to increase from 28 VDC to +/-270 VDC and may even continue to increase beyond this level throughout the coming years [1-3]. Increasing supply voltage levels are becoming more common. It leads to a reduction in the cross-section of electrical cables for the same power delivered. This has an impact both on costs and on the mass to be transported; this is particularly important in aeronautics. This tendency also relates to photovoltaic systems, smart grid systems and the telecommunications industry [4]. Many types of electrical defects are listed. Among these faults, electric arcs in series with the load are particularly difficult to detect accurately. They can be caused by a fault in the electrical connection or by accidental shearing that allows the arc to occur. In AC networks, the arc is extinguished at each half-wave when the voltage passes through zero. For DC sources in case of arcing faults, the probability of long-term maintenance of the arc is very high, making this type of fault extremely dangerous. Arcs can also occur parallel to the load. For these faults some protection devices based on current thresholds or differential analysis are effective in protecting the circuit. This is why the study presented in the following is mainly focused on the reliable detection of series arcs in a DC network consisting of a single power line. However, the solution can then be extended to parallel arcs. The predominant detection methods, aspresented in scientific literature, concern the diagnosis of DC faults in PV systems [5-13] including machine-learning techniques [14-23]. The first type of detection method depends upon athe temporal analysis of the electrical characteristics of the current. In some cases, it is based on the voltage delivered by the power supply (see the analysis of the variance proposed by [24]). In [55], the system for detecting series arcs relies on the identification of the voltage drop at the moment when the arc ignites. Other methods, such as the one proposed by [26], are based on a multi-criteria analysis of the line current in PV systems (the difference between the minimum, maximum and average values of the current and frequency analysis in a limited band of frequency). Authors in [27] proposed a differential current-based solution for a photovoltaic-based DC microgrid. The formula, used to calculate the entropy of the current passing through the panels, forms the basis of the criteria used for regulating the detection process [28]. [29] has proposed a method for detecting arc faults, that is based on HMM and wavelet analysis and is specifically designedfor use with DC networks. Most of the proposed methods are based on athe frequency analysis of the line current however. This type of analysis relates to the frequency bands whose content increases following the ignition of an electric arc. In [30], the authors have also proposed a detection method for DC SSPC (28V-supply voltage) and haveretained the bandwidth frequency [10Hz, 10kHz] in the case of inductive loads. In [31], theauthors analyzed the source of an arc-voltage noise and observed the variations that occurred within the three bandwidths [1-10kHz, 10-40kHz, 40-400kHz). The frequency band proposed for PV-DC arc detection was limited to [0.1-4kHz] for [26], [40kHz – 100kHz] for [32] but multiple frequencies [33-35]. T. Li and al. [36] proposed to compare two methods based on the current analysis which are the short time Fourier transform and the discrete wavelet transform associated to a convolutional network . The choice of the frequency bands was mainly dependent on the configuration of the circuit (multi-sources or combined loads) and on certain particular loads, such as switching loads. It is important to note that arc faults are strongly impacted by the type of loads present in the circuit As the bandwidth of the majority of switching converters is similar to that of arc-fault signals,

J. B. Humbert, P. Schweitzer, and S. Weber work at Jean Lamour Institute in team MAE (Measurements and Electronic Architectures), University of Lorraine, Nancy, France, e-mail: Patrick.schweitzerza@univ-lorraine.fr, serge.weber@univ-lorraine.fr.

these switching can be incorrectly interpreted as cases of arc faults and this increases the risk of false detect ions [37]. In order to reduce the rate of such false detections, the authors of [38-39] proposed a multi-band analysis linked to a statistical analysis.The use of a noise-reduction technique can eliminate disturbances in the process. It does so by removing the peaks in the current level linked to the switching frequencies. When authors of [33-35] presented a complex simulated circuit that considered 5 different DC/AC converters. they conclude that arc-fault detection can only be accomplished if it is possible to differentiate between the various peaks present in the frequency band of the switches. The detection method of [40] is based on a comparison of the magnitude of the line-current spectrum before and after the moment when a drop in the current is detected within the [10-70 kHz] bandwidth. The ongoing challenge that we face, is the need to develop a reliable detection method that continues to function correctly even in the presence of switching-supply sources or loads. The main difficulty we encounter relates to the fact that the spectral components for switching are superimposed onto the frequency band that belongs to the electric arc. Another problem is the fact that the switching frequencies (which we cannot know in advance) can vary widely from one load to another. We must therefore employ a detection process that is capable of completely overcoming the disturbance caused by frequencies that do not correspond to arc faults. In order to solve all of these problems, this paper will present a method for detecting the presence of series-arc faults, based on a frequency analysis of the line-current signature.

This paper will offer the following information:

• The process used for the detection of anomalies realized by using an indicator of frequencies, known as the SDI (Spectral Detection Indicator) obtained from the dynamic thresholding of the histogram.

• The confirmation of faults (in this case, a fixed number of anomalies occurring within a given time), through a process of counting up and counting down, whose principal advantage is that it is easy to implant into an on-board electronic circuit.

This paper will be presented as follows:

The first part will contain a description of the measuring test bench that consists of a continuous power source and a variety of linear and non-linear loads. This paper will also provide a complete database of current signatures that occur in the presence or absence of an arc fault will also be provided. Then, the strategy developed for the detection of series arcs that relies on the calculation of the Spectral Density Index (SDI) will be presented.

The second part will provide a description of the confirmation/decision block that activates the arc-time indicator (Trip) over a defined period of time.

In the final part, the results of detection processes used during tests undertaken on simple, nonlinear and switching loads will be presented.

## II. Signal Database

The algorithm used to detect arc faults was validated by referring to a current-signature database obtained using the experimental setup shown in Fig. 1. The load was tested under normal operating conditions and then in the presence of an arc fault. The subsequent current signatures were recorded. The experimental test bench made it possible to reproduce series-arc defects by opening contacts in a DC power line. The test used both obtained and copper electrodes (6.3mm) or carbon electrodes (6.3mm). The measurement of the arc voltage confirmed the presence of an arc fault.

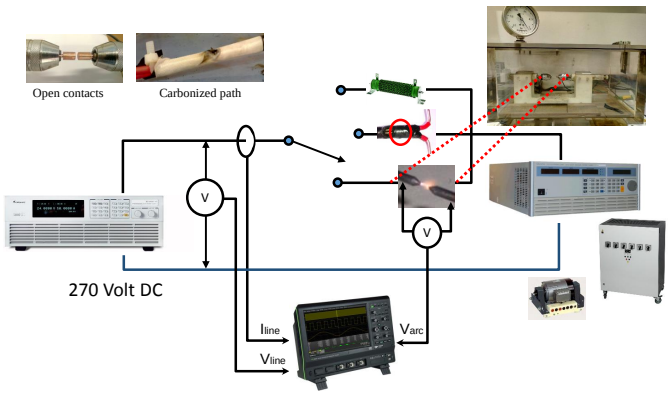


*Figure 1: Experimental test bench.*

Two different continuous and stabilized power supplies (270 VDC) can be used (CHROMA 62000H - ETSystem 3kW). The power line also includes linear loads as well as switching loads:

• A variable-resistance load (from 12 to 240Ω) with an inductance (between 30µH and 100µH).

• The CHROMA 63200 active load used as a variable resistor with electronic regulation (in power and current) then as an active load to reproduce a 500Hz inverter and a PWM type power regulation (1kHz switching frequency).

The ignition of an electric-arc fault in the line causes the current level to drop in a manner similar to that seen during a load change. An initial test was performed on each of the appliances that used a series arc in the power line as shown in Fig. 1. The electric arc was then replaced with a resistance of impedance (called 'lure') that had a level close to that of the electric arc. This duly caused the same drop in current level. In the first case, the detection algorithm must detect the presence of a fault. This will not be the case for the second configuration. The measurements were taken using a LECROY HDO4096 oscilloscope, at a sampling frequency of 1 MHz over a duration of 3 seconds. Measurements of line and arc voltages were made using the Testec TTSI9010 active-differential probe. The AP015 (Lecroy) current probe was configured to have a 100 Mhz (cal 0.1A) bandwidth. A database of line-current signatures (that occur when a series arc is present in the circuit) was compiled. It concerns both linear and switching loads and provides information regarding the following situations:

• 128 cases of arc faults occurring with linear-resistive loads (current between 2A to 22A)

• 10 cases of arc faults occurring with electronic loads (power regulation (1.5kW))

• 14 cases of arc faults occurring with electronic loads (current regulation (5.6A))

• 10 cases of arc faults occurring with an "inverter" type loads (2-10 Apeak 1kHz)

The compiled database consists of current signature results. Such current signatures occur during transients and alsoduring the switching and activation of loads that operate under conditions that do not produce arcs. Indeed all these situations can produce spectral changes and thus be the cause of false detections. The different tests performed were as follows:
• 145 cases of switching with the addition of a resistive load R (between 2A to 22A)
• 125 cases of switching using an electronic resistive load R (between 2A to 22A)
• 3 cases using an inverter load (2-10A and 1kHz switching frequency).

The current-signature database, used to evaluate the performance of the detection algorithm, contains a total of 435 current signatures. Of these current signatures, 162 were recorded when there was an arc fault present in the electric line and 273 were recorded in healthy conditions.
A link given in [41] gives access to the dataset of electrical current and voltage signatures which can be used under certain conditions.

## III. Arcing-fault detection based on the Spectral Density Index.

As previously mentioned, the arcing fault are non stationary and both their frequency and power spectra vary over time and many high frequency components are present in the currents of arc faults according to previous studies. To reveal the spectral content of the time varying arcing fault current signature, it is necessary to generate a representation of the current signal in the 2D space (time and frequency domains). The STFT base approach is selected in this work. Indeed, the STFT is a linear transform which also present the advantage of being a method which can be easily implanted in a embedded circuit. The calculated spectrogram will allow to visualize the energy distribution of the investigated faulty current signal in the time frequency plane. The fault features at every time instant can thus be detected and identified.

### A. Presentation of the detection method

Fig. 2 illustrates the proposed method for arc-fault detection, which includes an anomaly-detection phase followed by a decision step.

The spectrogram was calculated using the value the line current and which was then binarized [the threshold is noted Thbin]. In this section we will demonstrate the disadvantages of using a fixed threshold for all types of loads connected to the circuit. We preferred to rely upon adaptive thresholding instead. The Spectral Density Index (SDI) can then be calculated using data from the binarised spectrogram. A second thresholding technique (referred to as ThF), used on the SDI, permitted us to generate a signal that was capable of indicating the presence of anomalies of variable durations. The

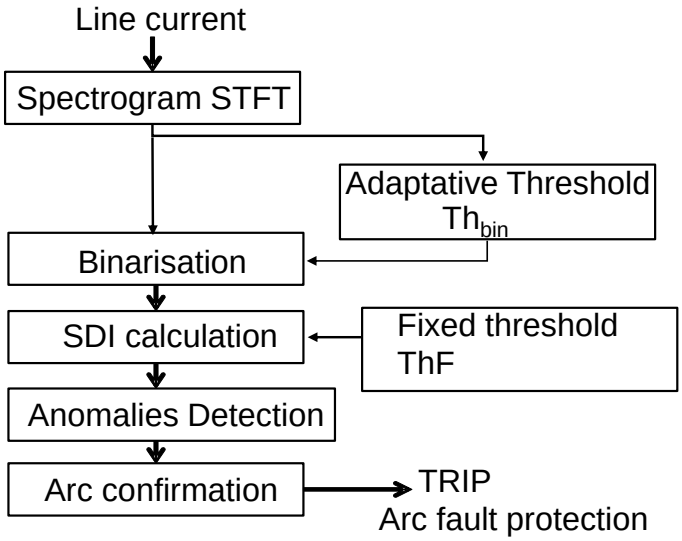


*Figure 2: Flow chart of the detection method.*

confirmation block, present during the last step of the process, is able to confirm the presence of an electric arc in the circuit. Regarding the detection principle employed in this study, a trip indicator (TRIP) is activated when cumulative anomalies remain present for a period of at least 10ms (over a 100ms sliding-analysis window).

### B. Frequency analysis of the line currents.

The Short-Time Fourier Transform (STFT) of a discrete time signal x[n] can be expressed by:

$$X(n,k) = \sum_{m=0}^{N-1} (x[m+n].w[n].exp(\frac{-j2\pi kn}{N}) \qquad (1)$$

N is used to represent the length of the window w[n]. n and k represent a time and frequency index. The performance of the STFT depend on:
• The type of function of the window
• The length (N) of the segments
• The overlap between the segments

During the application of our methods, the hamming window was chosen in order to minimize spectral leakage (Fig. 3). In order to ensure that all impulse information is taken into account by the spectrogram, the overlap ratio (from one window to another) must be equal to 1/2 the length of a window. For a window of width N, a maximum sliding window length of $\sigma = \frac{N}{2}$ must be chosen.

Fig. 3 shows the evolution of the current in a circuit using a 270-Volt DC supplying a linear resistive load. The selected window length was 4ms, the sampling frequency was Fs = 1MHz (Window Size 10kS). The frequency resolution was equal to 250Hz. The window coverage was set to 1ms in order to observe fast transient phases of up to 3ms without the risk that they would be truncated during the analysis. In our experimental test bench, the ignition of the electric arc was controlled by a switch. The action of this switch caused

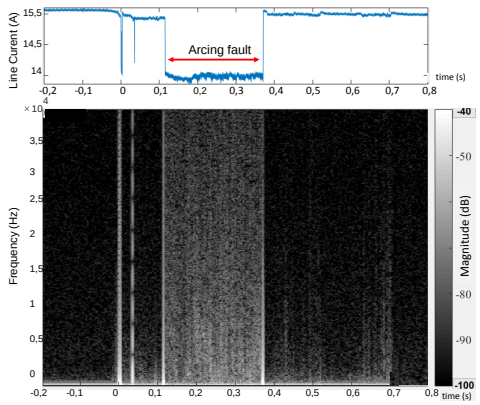


*Figure 3: Spectrogram of a single resistive load powered by a 270 VDC source (opening electrodes test).*

two interfering pulses in the line current at the time noted t = 0 in Fig. 3. An arc appeared at t = 0.1s causing an increase in the load impedance of the circuit (Zload + Zarc). This variation caused the current level to drop by 1A. The spectral content is weak during healthy situations but not totally equal to zero. In general, the level of noise in the circuit, where no faults occur, is strongly dependent on:

- The residual-noise level (related to the type of power supply) and the type of load or external disturbances (EMI - RFI interference).
- Disturbances that are naturally generated by switching loads.
- The performance of the measurement and acquisition systems.

A series arc causes current spectral content of the current to increase significantly due to its chaotic nature. The spectral content in the absence of arc fault is relatively low by contrast.

Performing the detection is more complex in the case of switching loads. Figure 4 represents the evolution of the line current (and the associated spectrogram for a 500Hz inverter) in the presence of an arc that was ignited at stage t=0s. The spectrum was characterized by the regular appearance of instantaneous frequencies. It was also the noted that mainly odd harmonics (related to the triangular shape of the signal) were observed at in this frequency range. The random content of the arc signal between t=0 and t=5s is superimposed on these fixed-frequency components.

It is particularly difficult to undertake detections in the case of polluting loads (for example: switching loads or inverters with high harmonic content). Without a precise knowledge of the switching frequencies specific to each device (the spectral content of the current being strongly disturbed in the absence of defects) this type of charge can cause a significant number of false detections. One solution is to limit the analysis for reduced-frequency bands (which do not include the load or supply-source switching frequencies). But in this case, the detection algorithm will only function reliably with these specific loads, however. In the following section of this article,

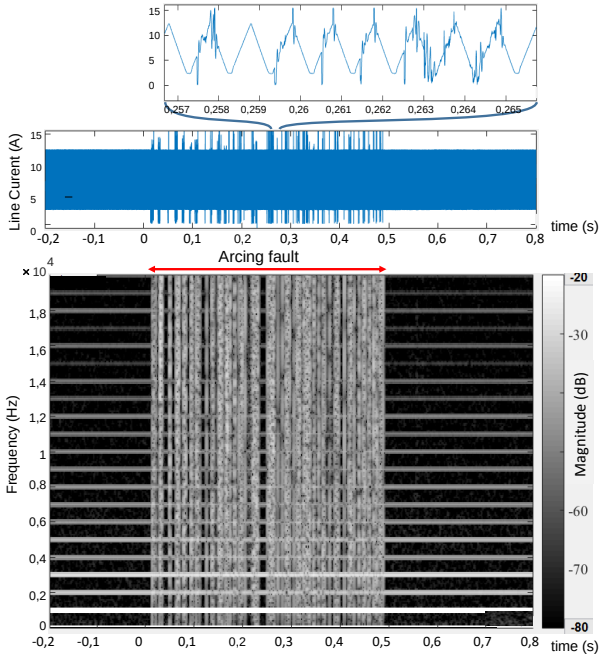


*Figure 4: Spectrogram for an inverser (0-10A). (Window size: 10kS, Spectral resolution: 100Hz).*

we will propose a detection method that is not dependent on this type of load and is resistant to the type of switching frequencies that are the sources of false detection. We have created an original solution which is able to calculate the Spectral Density Index. This makes it possible to estimate the degree of spectral spread in the line current. The method to estimate this index is described below.

### C. Spectral Density Index (SDI)

The Spectral Density Index was calculated using the spectrogram of the line current. The spectrogram X(n,k), calculated using Equation 1, was initially binarized according to the following equation:

$$bin(n,k) = \begin{cases} '1' \ if \ X(n,k) \geq Th_{bin} \\ '0' \ if \ X(n,k) < Th_{bin} \end{cases} \quad (2)$$

$Th_{bin}$ represents the binarization threshold.

In regards to the method chosen to analyze the frequency band, we relied upon results contained in literature and focused on a wide frequency band between 10kHz and 100kHz (chosen experimentally). The calculation of the Spectral Density Index was then calculated according to Equation 3.

$$SDI(n) = \frac{1}{N} \cdot \sum_{N} bin(n,k) \quad (3)$$

N represents the number of points of the selected frequency band. Fig. 5 shows the binarized spectrogram and the SDI calculation obtained by observing a circuit with a resistive load

[R=18 Ω - Vsupply = 270 VDC]. The binarization threshold Thbin was set to a constant value - 60dB. The SDI was only comprised of values between 0.8 and 0.9 in the presence of an electric arc (0.1 <t <0.38s). At stage t=0, the two peaks are created during the mechanical opening of a switch that is used to produce a series-arc fault in the electrical circuit.

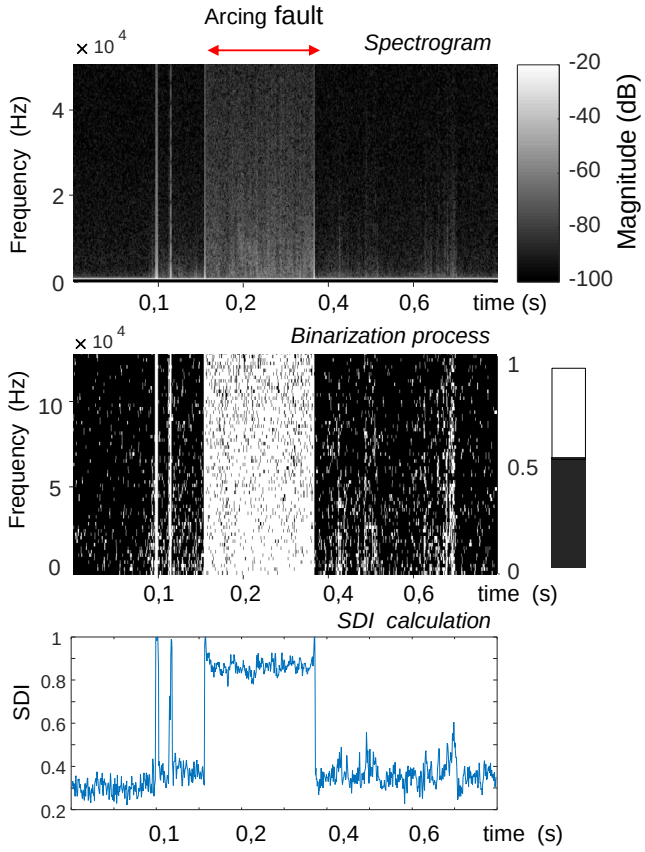


*Figure 5: Spectrogram and binarisation, FFT: 4096 points - Fs=1MHz*

The SDI was calculated based upon all of the signatures of the electric current that were generated when working with resistive loads (currents between 3.3 and 22 A). The set of results calculated for the threshold (constant value equal to -100 dB) is shown in Figure 6. The graph appears in the form of a (max - min - avg) chart. Fig. 6 shows us that the threshold of differentiation (in the range of 3.3A to 17A) cannot remain constant when we move between situations where an arc is, and is not present (ARC and NoARC).

As the line current grew weaker (approaching 3.3A), the average values of the SDI, that were obtained with and without arcs, became closer. The results also prove that, if the circuit does not contain an arc, the noise level predominates and the SDI value is close to 1. To overcome these drawbacks, it is possible to employ a dynamic threshold obtained by using a continuous estimation of the spectral content. The spectral content is calculated by employing a sliding window of observation to monitor amplitudes on a spectrum within a predefined range (Fig. 7).

By using this calculation it is possible to take into account,

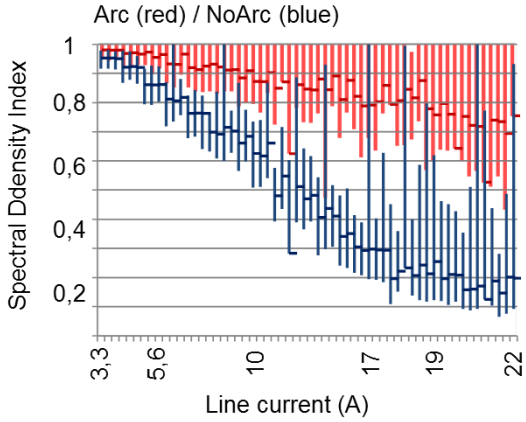


*Figure 6: The min-max chart of the SDI (static threshold: 100dB).*

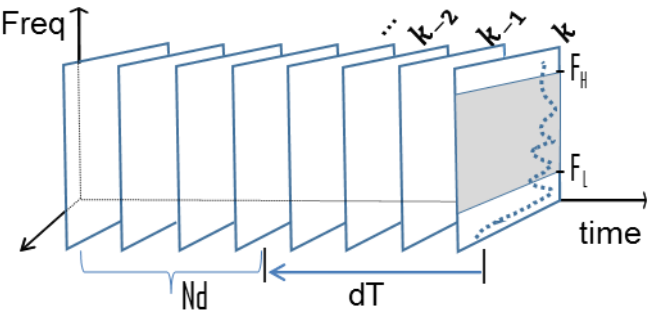


*Figure 7: The calculation of the Dynamic-binarization threshold using a sliding window.*

the average disturbances of measurements related to loads and power supply. This therefore limits the influence of the harmonic variations that occur due to nonlinear variations. Thus, the binarization threshold ($Th_{bin}$) is evaluated continuously considering a window of duration Nd time-delayed by a time noted dT according to Equation 4.

$$Th_{bin} = \frac{1}{Nd.(f_H - f_H)} \sum_{n=0}^{Nd} \sum_{f=f_L}^{f_H} X(n - dT, f) \quad (4)$$

Fig. 8 shows the results of the SDI estimation versus line current that were recorded using the adaptive thresholding presented previously. The values of the average levels contained in the SDI (that occurred during the two events referred to as 'Arc' or 'No-Arc') are well separated for all the current values between 3.3A up to 22A. The SDI values range from 0.3-0.4, when no arc occurs in the line, and from 0.6-0.9 when there is a serial fault in the circuit. By choosing an optimal threshold (as seen in the threshold range in Fig. 8) two distinct classes (Arc and NoArc) are distinguished.

### *D. The detection of anomalies*

Fig. 9a represents the evolution of the current in a circuit composed of a DC source supplying a resistive load. When an arc is produced in series in the circuit, the current drops. The two pulses that appear at time t=2s correspond to the switching

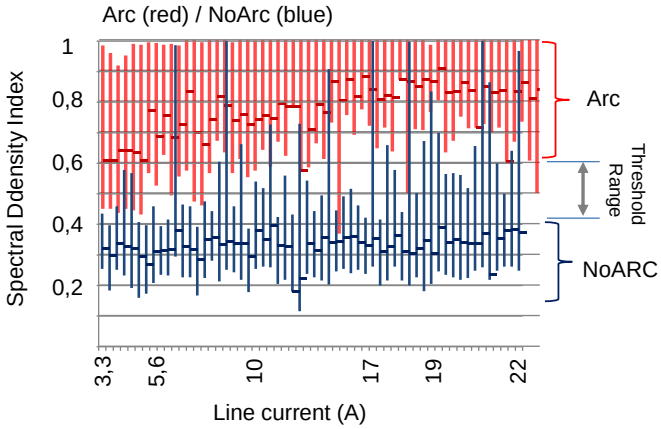


*Figure 8: The min-max-mean chart of the SDI (Auto-adaptative threshold) Nd=10ms, dT=100ms*

of a relay that makes the arc active. In regards to the current, the evolution of the SDI level is represented on Fig. 9b. The switching of the relay and the arcing fault, as well as the abrupt changes of the current, cause a significant increase of the SDI level. Its thresholding in accordance with the parameters of Equation 5 gives a binary signal ($detect_{an}$) (In Fig. 9c, the threshold is arbitrarily set to 0.6 for this test). The two-state binary detection signal is set to 0 when no anomaly is detected and 1 when an anomaly is detected.

$$detect_{an} = \begin{cases} '1' \ if \ SDI(n) \geq Th_F \\ '0' \ if \ SDI(n) < Th_F \end{cases} \quad (5)$$

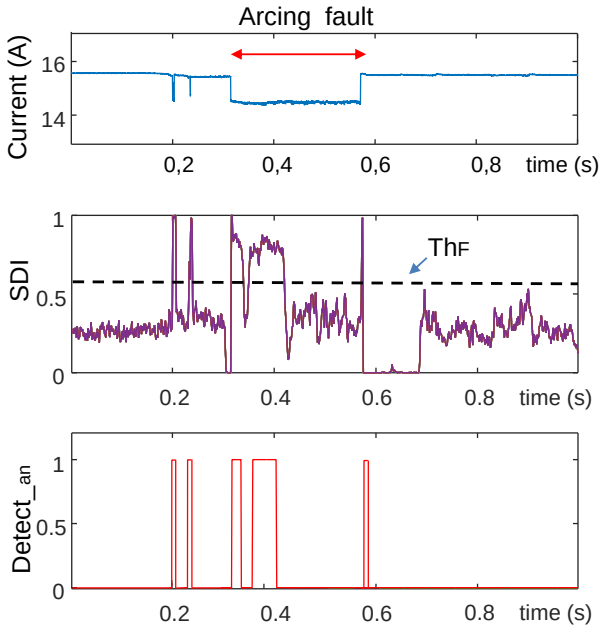


*Figure 9: Current line, SDI and anomalies indicator versus time for a resistive load.*

### *E. Optimal threshold for anomalies detection*

At this stage, the value of the binarization threshold (ThF) was chosen experimentally. The experimentation process was based on the understanding that the detection method should operate at the optimum level regarding on all of the different loads that could be connected to the circuit. To this extent, we will define the evaluation of the performance of the detection criterion in terms of sensitivity, sensibility and accuracy. This will be done using a method, widely used in other scientific fields, that depends upon the calculation of the confusion matrix [44]. In this work, a set of experimental test situations (True) that combine operating modes both with arcing faults (Faults) and in normal operation (No Fault) is reproduced. The classified results of the detection methods (predicted class) are divided between arc faults (Fault detected) or normal situations (No Fault detected), based on the results obtained by calculating the SDI for the test dataset The confusion matrix (Tab. 1) combines the classification results and includes 4 categories. The acronyms 'TP' and 'TN' represent cases that were correctly classified whether they were positive or negative. 'FN' and 'FP' represent the number of occasions where negative and positives cases were incorrectly classified [42-46].

The performances were estimated in terms of:

- Sensitivity (true positive rate)

$$TPR = \frac{TP}{TP + FN}$$

- Specificity (true negative rate)

$$TNR = \frac{TN}{FP + TN}$$

- Accuracy

$$ACC = \frac{TP + TN}{TP + FP + TN + FN}$$

The accuracy value relates to the proportion Number of truly positive responses out of the total number of responses.

The best conditions for ensuring optimal detection rates occur when the value of the specificity is low and value of the sensitivity is high.

The optimum setting of the ThF threshold must be sought so that the detection is effective for all the loads present in the circuit. An experimental analysis of all the curves representing the SDI as a function of time has led us to say that this optimum threshold is between 0.4 and 0.6. In a first step, the performance values (specificity, sensitivity and accuracy) are calculated using the three detection values for ThF (0,4-0,5-0,6) taken from all signals in the database (270 situations without arcing defects and 128 with arcing defects). The results are presented in Tab.I. The performances are close for the three threshold values.

*Table I: Detection performances for different values of ThF.*

| ThF | 0.4 | 0.5 | 0.6 |
|---|---|---|---|
| Specificity% | 26 | 28 | 36 |
| Sensitivity% | 100 | 100 | 98 |
| Accuracy% | 50 | 51 | 56 |

In regards to the three values of the threshold, a sensitivity close to 100% represents a very good detection rate. A certain number of detections are erroneous however (26% <specificity <36%) and a good detection rate can be considered to be just over 50% (50% <accuracy <56%). Although the number of false detections may seem significant, such occurrences mainly appear during the transitions of loads or transients. They will be eliminated during the confirmation/decision stage. In a second step, Fig. 10 shows the SDI values obtained for different loads where arc faults were, and were not, present. The average values are distinct in the vast majority of cases (inverters, power regulators, active and resistive loads, inductive loads and PWM, for example). However, in the case of the inverter and the power regulator, values on the extreme ends of the spectrum became superimposed and this lead to the occurrence of false detections. By contrast, in the case of highly inductive loads, the average IDS obtained during situations that did , and did not, feature an arc fault in the line share close values. Given this context, we can already state that it will be difficult to choose the type of separation threshold between the two states (with and without an arc), that will provide the optimal rate of detection.

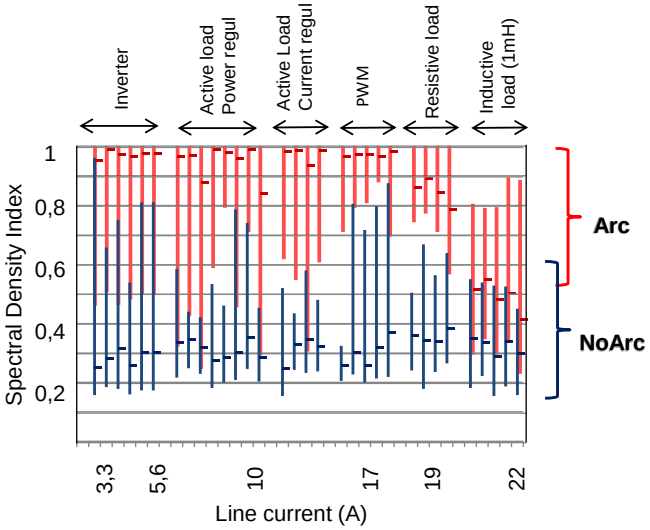


*Figure 10: The SDI for different domestic appliances.*

For the information presented in the following section, and in accordance with the results presented in Tab. 1 and Fig. 10, the threshold value of the SDI is fixed at 0.5. This value is a good compromise to guarantee good performances of detection.

Fig. 11 represents the evolution of the SDI in regards to a switching load, whose spectrogram is represented in Fig. 5. During normal operation, the SDI level is low (close to 0.2) and remains almost constant. The switching frequencies do not disturb the proper functioning of the binarisation algorithm. The SDI values show very high variability over time in the presence of an arc fault in the circuit, however. It is often possible to attain the maximum values. In conclusion, the thresholding of the SDI (ThF) = 0.5) provides a binary signal that indicates the fact that an arc fault has been detected when one occurs. Then, a logic of decision is implemented to confirm the presence of an anomaly from using preselected detection rules.

The confirmation block is responsible for activating an indicator (noted as 'TRIP') that signals signal the presence of an electric arc. This signal can be used to open the circuit after the arcingfault is confirmed. The procedure followed in this block is similar to the one proposed for the anomaly-detection process used for real-time serial communication buses (LIN, CAN, VAN, FLEXRAY).

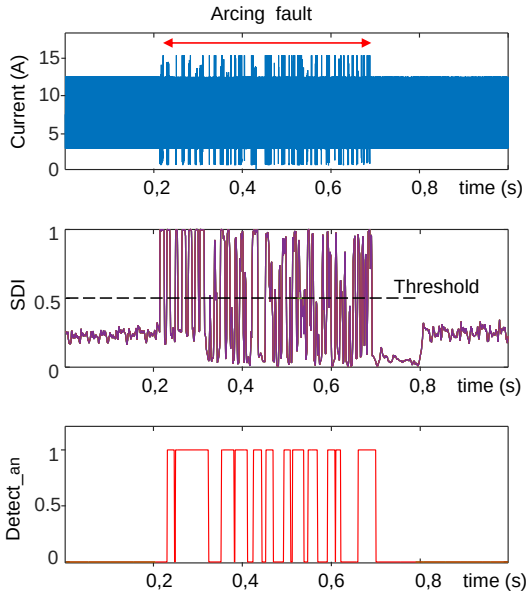


*Figure 11: Current line, SDI and anomalies indicator versus time for a switching load.*

### F. Decision bloc – TRIP activation

In the course of this study, the following rule was adopted: a TRIP indicator was activated when a cumulative sequence of detection (given by the Anomalies detection indicator), lasting 10ms, was undertaken over a period of 100ms. Fig. 12 shows a state diagram which illustrates the operating mode. The states are represented by circles and the arrows are related to the possible transitions between states.

At the beginning of the cycle, the machine remains in State 0 (the normal mode of operation), during the period where no faults are detected (which corresponds to $\overline{detec_{an}}$). The machine will transition into State 1 if the opposite scenario ($detec_{an}$) occurs. The TRIP Indicator will display the value '1'. The method of indication resembles a 'counter' device.

The value of the counter rises by the value 'a', as soon as an anomaly is present in the circuit. It continues in the same manner after each cycle of analysis. By contrast, the value of the counter falls by value 'b' during each iteration. As soon as the value of the counter exceeds that of the threshold (set to a fixed value L1) the indicator that responds to the presence of an arc (TRIP) is activated. Fig. 13 illustrates the operating mode of the anomaly-detection and arc-confirmation stages that were obtained using the different values of a, b

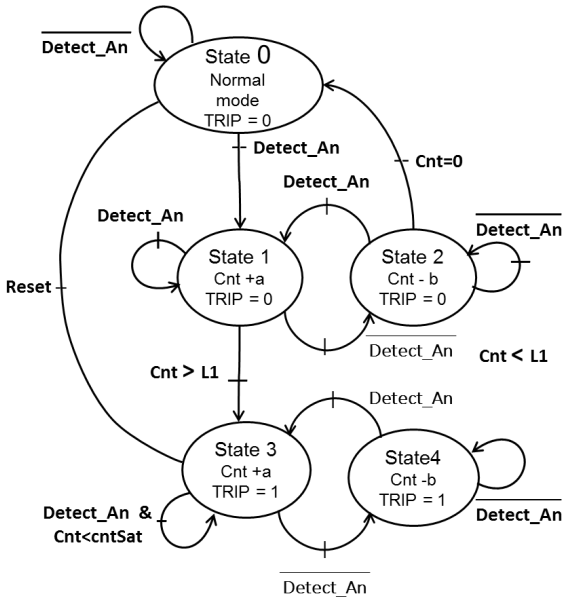


*Figure 12: A diagram of the state machine for a decision part of the process.*

and L1 (the value of L1 was fixed at 100 through a process of experimentation). Figure 13a corresponds to the pattern of random-fault detection obtained when arc faults do not continue for a sustained duration (between 0 and 150ms), 11 faults were detected and the arc appeared sporadically in the circuit. Beyond 250ms, the anomaly detection is maintained at level 1 indicating the presence of a permanent disturbance.

In Fig. 13b, the electric arc is barely noticeable between 0-150ms and is detected as soon as it appears. Although the conditions conducive to the appearance of a fault are met during the analysis window (10ms over 100ms), the settings of parameters 'a' and 'b' (a = 10, b = -0.6) do not allow a fault to be detected. When the arc fault continues for a sustained period (from t = 250ms), the detection process becomes operational and it takes 10ms to put the Trip Indicator into State 1 A second adjustment of the parameters a and b, made it possible to achieve a strong increase and low decrease of the counter (a = 20, b = -1).

Fig. 13c shows that the TRIP indicator is triggered as soon as a fault appears, during a cumulative duration or 10ms that occurs over a period of 100ms. At t = 148ms, the TRIP indicator returns to a low-level (inactive) state which is not the case for a conventional circuit breaker. Indeed, in order to study the proper functioning of the detection algorithm, the TRIP indicator is regularly reset. Then, as soon as the fault is continuously detected (t> 250ms), the TRIP indicator is activated in less than 10ms (Fig. 13c). In the case of temporary arc faults, that vary in duration and are analogous to a false contact (loose terminal test), the evolution of the line current is represented by the curve shown in Fig. 14a. The test is performed on a resistive load supplied by a 270-VDC source. The detection rate can be also be considered to be efficient when this configuration is employed and faults only occur intermittently. These types of phenomena, that are related to spontaneous arcs, correspond to false or even random contacts of variable frequencies and duration. The evolution of the TRIP indicator (blue bar) and the plot of the meter (green) are shown in Fig. 14b. The results presented in Fig. 14 show that detection is performed perfectly when monitoring random defects.

Fig. 15 shows how we plotted a curve representing the cumulative length of arc duration from the point where the first anomaly is detected. At t = 525ms, when the first fault is detected, the counter can register the presence of transient faults and its value subsequently increases (blue curve). In the absence of a fault, the counter value starts to fall but much more slowly. When the anomaly persists for over 10ms, the protection process is activated as shown in Fig. 15. The tripping time can be perfectly adapted to other specifications by adjusting parameters 'a' and 'b'. The red curve shows a case, during which the activation of the TRIP signal almost doubled.

## IV. Results

Fig. 16 shows a ROC curve that was plotted using data related to sensitivity versus specificity. It shows results for all resistive loads, both with and without the decision block. The IDS threshold ThF evolved from 0.1 to 0.9 for the following parameters of adjustment of the decision block (a = 10 and b = -1).

By reading the data contained in the ROC curve, it is possible to determine the optimum threshold necessary for obtaining the best possible detection rate (i.e.: a 100% sensitivity level and a 100% absence of detections for healthy cases). Such results were obtained when the ThF level is equal to 0.5 (green line). Without the decision block, the best performances were obtained when the ThF level was = 0.9 (blue line). In this case, the specificity reaches 70% (which is to say there will be a 30% level of error in regards to healthy cases). The rate of good detections was 82%. The addition of the confirmation/decision block considerably increased the rate of correct detections and conversely minimized the rate of false detections.

*Table II: Confusion Matrix for all electrical appliances.*

| | TP | TN | FP | FN | ACC) |
|---|---|---|---|---|---|
| Resistive load | 128 | 270 | 0 | 0 | 100% |
| Inverter Load | 8 | 3 | 0 | 2 | 80% |
| Active Load power regul | 10 | 0 | 0 | 0 | 100% |
| Active Load current regul | 13 | 0 | 0 | 0 | 87% |

Thus, for a threshold of ThF=0.5, 100% efficient performance is obtained for situations with and without an arc fault. The detection algorithm was also tested on all ofthe current signatures in the database (the R load, Inverter and Regulator). The results are shown in Tab. II. The results presented in Tab. 2 demonstrate that the rate of correct detections is quite efficient and can reach up to 93% - 100% when used on resistive and regulated power loads. The worst performance, in terms of obtaining results, occurred when testing switching loads (Regul inverter). In this case the rate of correct detections falls

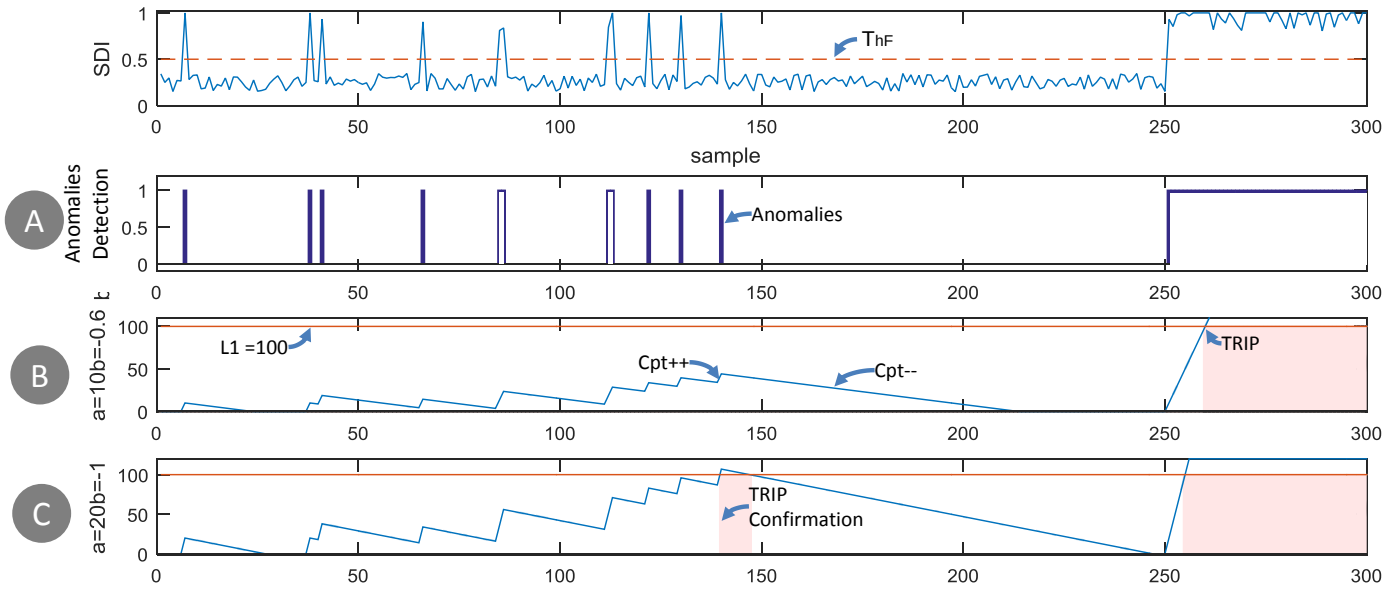


*Figure 13: Residuals (The result of the confirmation block analysis)*

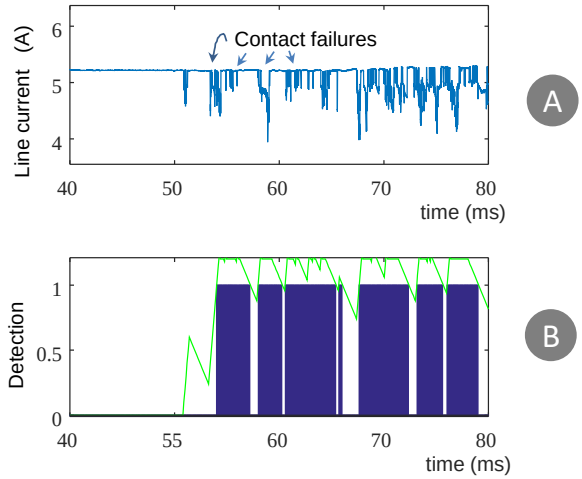


*Figure 14: Loose terminal test.*

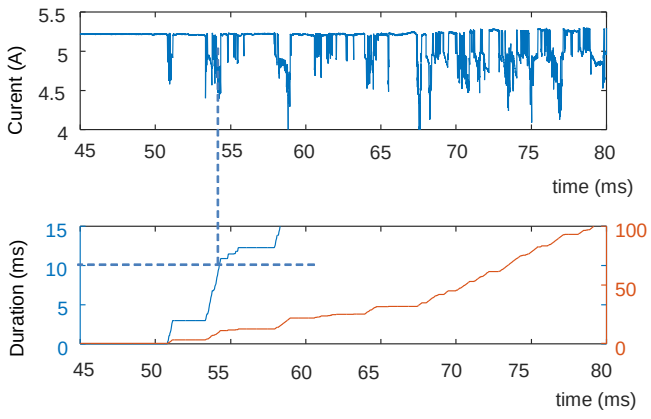


*Figure 15: Arc duration results*

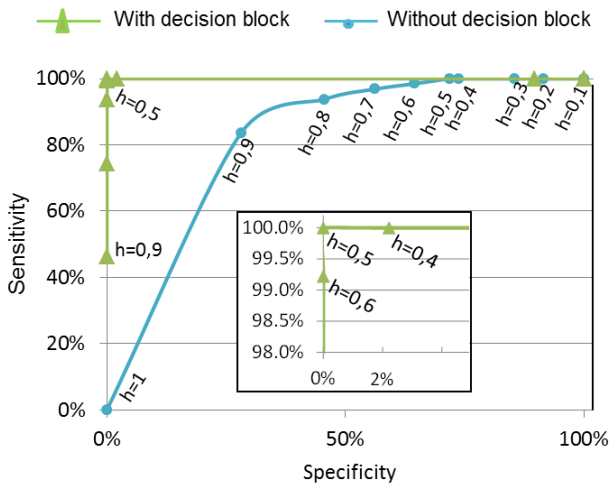


*Figure 16: ROC curves - Specificity versus Sensitivity*

to 80%. It should be noted, however, that for all the loads (FP = 0), no erroneous detection occurs and no nuisance tripping is observed. Fig. 17 shows the results obtained after the detection algorithm was applied to 6 different load configurations. The current signatures were placed end-to-end. The form taken by the currents, that were registered, is represented in Fig. 17a. The arc ignition causes the current level to drop in the case of a resistive load (segment VI  VII). The presence of the electric arc produces a strong variation in the spectral content, which in turn, causes the SDI to vary significantly. The detection of a series arc in the resistors (5A and 20A) is ensured (Trip = 1 Fig. 17c). Current disturbances related to the electric arc are significantly attenuated if the load becomes inductive (Segment V: L = 1mH and I = 8A). In this case, we witness the smoothing of the current by an inductive effect.

It should be noted, however, that the value of the inductance

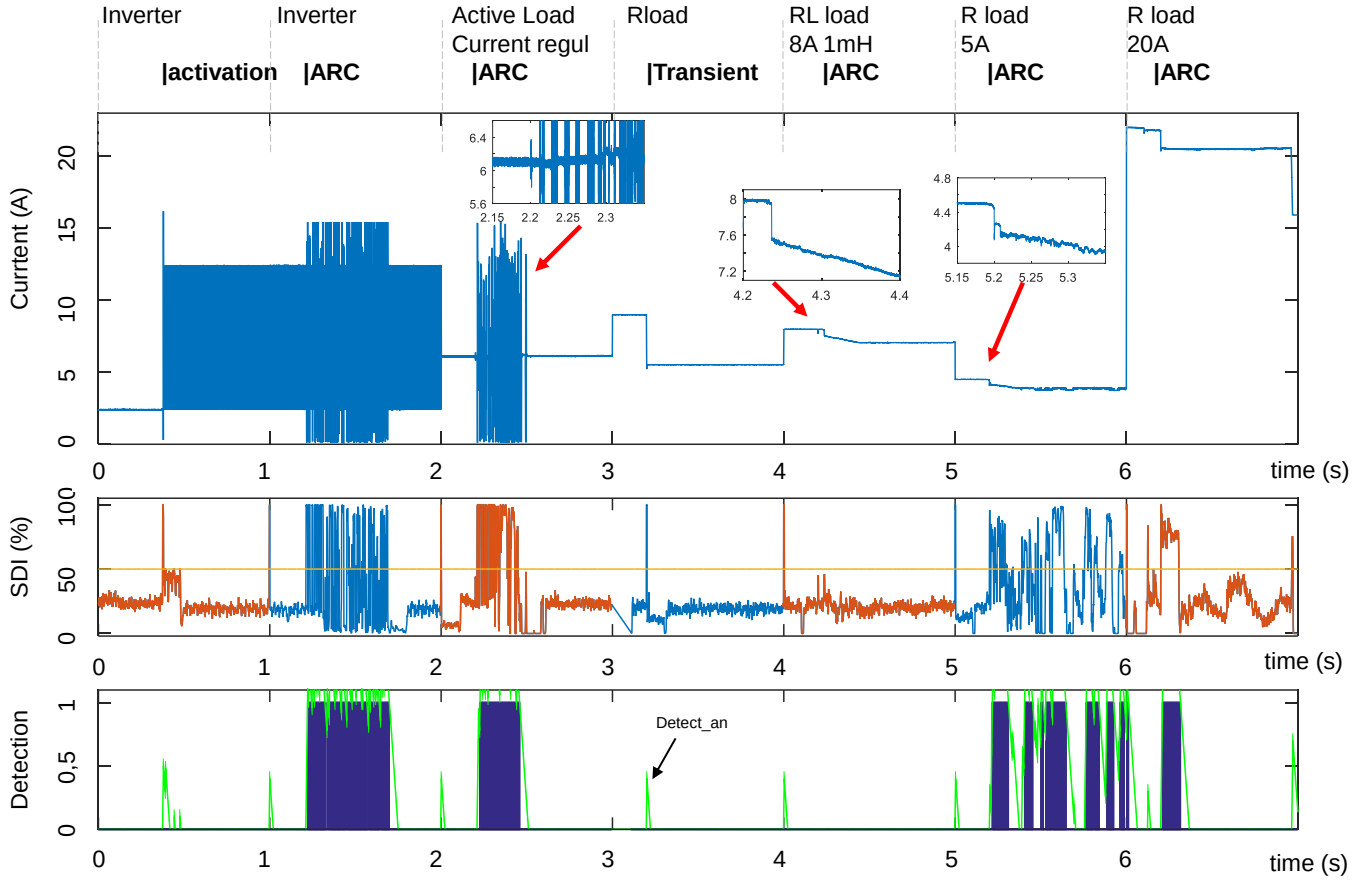


*Figure 17: Residuals (The detection performance of 6 different configurations (signal merged))*

is quite important (i.e.: 1 mH). This is not the case for traditional electrical loads.

If a variation in the level of resistance (Segment IV) resulted in the current passing from 20A to 50A, the device did not detect a fault and the Trip remained in a low state (no false detection). In the case of an inverter load (Segments I and II), the presence of switching frequencies did not cause false detections and the detection of arc faults could be executed perfectly. The Trip indicator remains in a low state during a faultless operation. On the other hand, when arc faults are present, when arc faults are present however, the arc disturbances are superimposed onto the current of the inverter (the value of the SDI remains weak, see Fig. 17c). These disturbances are detected by the apparatus and thus, the detection of an arc fault is guaranteed. In the case of a power regulator (see Segment III), the detection of a fault is also perfectly assured Trip = 1 (Fig. 17c). The switching of the load results in a peak in the SDI level (Fig. 17b). The duration is relatively short, however, and the detection process remains undisturbed as the binarization threshold of the spectrogram is dynamically adjusted.

## V. Comparison with existing methods

Tab. III. presents a comparison of our method with some related methods in recent literature (aspects such as the principle of the method, detection performances, type of load and domain of application). Above all, it should be noted that all the methods are applied for the detection of serial arc faults in a DC electrical network.

It is important to note that all of the detection methods presented in Tab. III are based either on a frequency analysis like our method or on the extraction of features both in time and frequency domain. In terms of detection performances, the proposed method gives satisfactory results which are comparable with those presented in Tab. III. Test results presented in [23] show that IntelArc method can detect accurately faults across 270 and 28 VDC levels and different forms of reactive loading. Nevertheless, this preliminary testing give good results on a limited number of scenarios and must be generalized to develop an AFD system. Authors in [8] uses a data acquisition system with a high sampling rate which can be an constraint to the implementation in an embedded circuit. Also, the complexity of computation is also is a constraint in terms of implementation in embedded electronics. The major methods presented in table xx are based on neural networks approaches which require a large amount of data, especially for network training. Contrary to the methods of the literature, the decision stage presented in this article is relatively simple and can be easily implemented, but above all gives very satisfactory detection results.

*Table III: Comparison of the proposed method with recently proposed approaches.*

| Ref | Fault detection method | Domain of application | Loads | Remarks | Performances |
|---|---|---|---|---|---|
| [36] | Time frequency analysis of the current (STFT and DWT) and CNN | Detection in all electrical aircraft DC source | Adjustable load | Need to train the CNN 3-5 times by using the training database. | Detection accuracy near 100 %. Detection time : STFT (0,5s) DWT (less than 0,2s) |
| [8] | Spectrum integration difference | DC networks 0-270 Volts DC Tests with one or two cables (300 meters length) | Resistive load, incandescent lamp, inverter, fan. | Current measurement through two capacitors. Oscilloscope :sampling rate 200MHz | Single cable : localization with a few meters Two cales : Localization error = 5,4% |
| [23] | Time and frequency domain features analysis + hiden Markov model | Low voltage microgrids within an aircraft or shipboard system | Case 1 : 270 and 28 VDC, Inductive and capacitive loads Case 2 : 33 and 28 VDC, Arc fault in a source feeder. | Case 1 : 60 model simulations. Preliminary testing of the algorithm | Case 1 : Diagnosis accuracy 98,3% Case 2 : Accuracy 100% (2 tests) |
| [22] | Time (Range, sum of absolute value, DC drop) and freq domain | Photovoltaic system | Cable : 45 meters PV panels and Inverter | Experimentation with one type of converter | Detection rate : 100%, 80 sets of experimental data |
| SDI | Spectrogram STFT + SDI calculation | Low power network. 270 VDC | Resistive and inductive loads Active loads | Adaptative threshold on the spectrogram | Detection accuracy between 87% and 100% |

## VI. Conclusion

This paper has presented a method for detecting series-arc faults in DC electrical networks, using a system based on the process of analyzing the line current. The method of arc-fault detection that we propose comprises two main steps: detection and decision. The results of our tests show that one of the most effective ways to detect an arc fault is to use a process based on an STFT analysis of the line current (i.e.: as soon as an abrupt change of current occurs). The binarization of the spectrogram (undertaken using dynamic thresholding) makes it possible to calculate the SDI that quantifies the dispersion of the spectrum of the current. The process of dynamic thresholding depends upon the regular recalculation of the spectrogram binarization threshold during a sliding window of analysis. The main advantage of this method, is that this threshold is automatically adjusted according to the different loads, disturbances or noise levels present in the circuit. The decision logic, based on a process of counting up and counting down the anomalies, confirmed the presence of an arc fault (such arcs were present for 10ms during a window that had a total duration of 100ms) and activated the Trip Indicator. One of the major advantages of using a decision block is that it can be easily integrated into an embedded electronic circuit. The algorithm has been tested using a database that consists of more than 400 current signatures. These signatures were obtained during both normal operational conditions and in the presence of a series arc, using resistive, inductive and switching loads. The performance level of the detection method is displayed in a confusion matrix. The algorithm is capable of differentiating a situation where an arc fault is present in a circuit, from one with no faults. This detection method performs very well. The results we have obtained demonstrate that switching loads do not lead to false detections. Cases where arc faults were not successfully detected occurred when working with inductive loads. Such loads cause a smoothing of the current which thus reduces the possibility of successfully detecting faults. Despite this, no false detections were identified in the case of any of the tests we performed. We can also consider making improvements to the process, including optimizing the frequency-band analysis (which ranged from 10 kHz to 100 kHz in this study). It is our conclusion that this frequency band can probably be reduced in scope, without negatively affecting the quality of its performance. By reducing the extent of the range of analysis, it will subsequently be possible to reduce the computing times required to implement the process in embedded electronic architecture.

## References

[1] X. Roboam, "New trends and challenges of electrical networks embedded in more electrical aircraft", in: IEEE International Symposium on Industrial Electronics, (2011), pp. 26-31.

[2] K. Niet al., "Electrical and Electronic Technologies in More-Electric Aircraft: A Review," in IEEE Access, vol. 7, pp. 76145-76166, 2019, doi: 10.1109/ACCESS.2019.2921622.

[3] B. Rahrovi and M. Ehsani, "A Review of the More Electric Aircraft Power Electronics", in: Power and Energy Conference (TPEC), 2019, pp. 1-6, doi: 10.1109/TPEC.2019.8662158.

[4] M. Fendrychova, P. Fiedler. "Challenges in Arc Fault

Detection for High Power DC applications", in: IFAC, Science Direct, 49-25 (2016), pp. 552–556.

[3] S. R. Madeti, S.N. Singh. "A comprehensive study on different types of faults and detection techniques for solar photovoltaic system", in: Solar Energy, 158 (2017), pp 161–185.

[5] S. Lu, B.T. Phung, D. Zhang. " A comprehensive review on DC arc faults and their diagnosis methods in photovoltaic systems", in: Renewable and Sustainable Energy Reviews, 89 (2018), pp 88-98.

[6] AE. Lazzaretti , CHC. Costa, MP. Rodrigues, GD Yamada, G. Lexinoski, GL. Moritz GL, E. Oroski, RE. Goes, RR. Linhares, PC. Stadzisz, JS. Omori, RBD. Santos. "A Monitoring System for Online Fault Detection and Classification in Photovoltaic Plants", in: Sensors (Basel). 17 (2020), pp 4688.

[7] E. Garoudja, F.Harrou, Y. Sun, K.Kara, A. Chouder, S. Silvestre. "Statistical fault detection in photovoltaic systems", in: Solar Energy,150 (2017), pp. 485-499.

[8] Q. Xiong, S. Ji, X. Liua, X. Feng, F. Zhang, L. Zhua, A. L. Gattozzib, R. E. Hebnerb, "Detecting and localizing series arc fault in photovoltaic systems based on time and frequency characteristics of capacitor current", in: Solar Energy, 170 (2018) pp.788–799.

[9] S. Lu, B.T. Phung, D. Zhang. "A comprehensive review on DC arc faults and their diagnosis methods in photovoltaic systems", in: Renewable and Sustainable Energy Reviews, 89 (2018), pp. 88–98.

[10] S. R. Madeti, S.N. Singh. "A comprehensive study on different types of faults and detection techniques for solar photovoltaic systemv, Solar Energy, 158 (2017), pp. 161–185.

[11] A. Mellit, G.M. Tina, S.A. Kalogirou. "Fault detection and diagnosis methods for photovoltaic systems: A review Renewable and Sustainable Energy Reviews", in: Renewable and Sustainable Energy Reviews, 91 (2018), pp. 1–17.

[12] D. S. Pillai, N. Rajasekar. "A comprehensive review on protection challenges and fault diagnosis in PV systems", in: Renewable and Sustainable Energy Reviews, 91 (2018), pp. 18–40

[13] I. M. Karmacharya, R. Gokaraju. "Fault Location in Ungrounded Photovoltaic System Using Wavelets and ANN, in: IEEE Transactions on power delivery, 33 (2018).

[14] A. Mellit, S. A. Kalogirou. "Artificial intelligence techniques for photovoltaic applications: A review", in: Progress in Energy and Combustion Science, 34, (2008).

[15] N. Qu, J. Chen, J. Zuo, J. Liu. "PSO–SOM Neural Network Algorithm for Series Arc Fault Detection", in: Advances in Mathematical Physics, (2020).

[16] J. E. Siegel, S. Pratt, Y. Sun, S. E. Sarma. "Real-Time Deep Neural Networks For Internet-Enabled Arc-Fault Detection", in: Engineering Applications of Artificial Intelligence, (2018).

[17] B. Basnet , H. Chun, and J. Bang. "An Intelligent Fault Detection Model for Fault Detection in Photovoltaic Systems", in: Journal of Sensors, (2020).

[18] A. H. Omran, D. M. Said, S. M. Hussin, N.Ahmad, H.Samet. "A novel intelligent detection schema of series arc fault in photovoltaic (PV) system based convolutional neural network", in: Periodicals of Engineering and Natural Sciences, 8.3 (2020), pp.1641-1653,

[19] F. Aziz, A. Ul Haq, S. Ahmad, Y. Mahmoud, M. Jalal and U. Ali. "A Novel Convolutional Neural Network-Based Approach for Fault Classification in Photovoltaic Arrays," in: IEEE Access, 8 (2020) , pp. 41889-41904.

[20] V. Le and X. Yao. "Ensemble Machine Learning Based Adaptive Arc Fault Detection for DC Distribution Systems,", in: IEEE Applied Power Electronics Conference and Exposition (APEC), 2019, pp. 1984-1989,

[21] M. Chen, X, Liu, Y, H, Chen, S, Gao, L, Zhu and L, Li. "Detection method of low voltage series DC arc based on the pattern matching algorithm", in: 20th International Conference on Electrical Machines and Systems (ICEMS), (2017), pp. 1-4.

[22] F. Jia, L. Luo, S. Gao, J. Ye. "Logistic Regression Based Arc Fault Detection in Photovoltaic Systems Under Different Conditions, in: Journal of Shanghai Jiaotong (Science), 24 (2019) pp 459-470.

[23] R. D. Telford, S. Galloway, B. Stephen and I. Elders. "Diagnosis of Series DC Arc Faults—A Machine Learning Approach", in: IEEE Transactions on Industrial Informatics, 13(4) (2017), pp. 1598-1609.

[24] F. Schimpf, L. Norum. "Recognition of electric arcing in the DC-wiring of photovoltaic systems", in: 31st International Telecommunications Energy Conference (INTELEC), (2009), pp. 1-6

[25] L. Mackay, A. Shekhar, B. Roodenburg, E. L. Ramirez, P. Bauer. "Series arc extinction in DC microgrids using load side voltage drop detection", in: IEEE First International Conference on DC Microgrids (ICDCM), (2015), pp. 239–244.

[26] Y. Gao, J. Zhang, Y. Lin, Y. Sun. "An innovative photovoltaic DC arc fault detection method through multiple criteria algorithm based on a new arc initiation method", in: IEEE 40th Photovoltaic Specialist Conference (PVSC), (2014), pp. 3188-3192.

[27] S. Dhar, R. K. Patnaik, P.K. Dash. "Fault Detection and Location of Photovoltaic Based DC Microgrid Using Differential Protection Strategy", in: IEEE Transactions on Smart Grid, 9.5 (2018), pp. 4303-4312.

[28] N. L. Georgijevic, M. V. Jankovic, S. Srdic, Z. Radakovic. "The Detection of Series Arc Fault in Photovoltaic Systems Based on the Arc Current Entropy", in: IEEE Transactions on Power Electronics, 31.8 (2016), pp. 5917–5930.

[29] R. D. Telford, S. Galloway, B. Stephen. "Diagnosis of Series DC Arc Faults—A Machine Learning Approach", in: IEEE Transactions on industrial informatics, 13(4) (2017), pp. 1698-1609.

[30] Meng Xie and al. "Arc fault detection for, DC solid state power controllers", in: IEEE Conference and Expo Transportation Electrification Asia-Pacific (ITEC Asia-Pacific), (2014), pp. 1-6.

[31] M. Wendl, M. Weiss, F. Berger. "HF characterization of Low Current DC Arcs at Alterable Conditions", in: The 27th International Conference on Electrical Contacts (ICEC), (2014), pp. 1-6.

[32] B. Novak. "Implementing arc detection in solar applications: achieving compliance with the new UL 1699B Standard". Texas Instruments, (2012).

[33] J. Johnson, S. Kuszmaul, W. Bower, D. Schoenwald "Using PV module and line frequency response data to create

robust arc fault detectors", in: Proc. 26th European Photovoltaic Solar Energy Conference and Exhibition Hamburg, (2011), pp. 3745-50.

[34] J. Johnson, C. Oberhauser, M. Montoya, A. Fresquez, S. Gonzalez and A. Patel, "Crosstalk nuisance trip testing of photovoltaic DC arc-fault detectors," in: 38th IEEE Photovoltaic Specialists Conference, Austin, TX, (2012), pp. 001383-001387

[35] J. Johnson, J. Kang. "Arc-Fault Detector Algorithm Evaluation Method Utilizing Prerecorded Arcing Signatures", in: 38th IEEE Photovoltaic Specialists Conference (PVSC), (2012), pp. 001378-001382.

[36] T. Li, Z. Jiao, L. Wang, Y. Mu, "A Method of DC Arc Detection in All-Electric Aircraft", in: Energies, 13 (2020), pp. 4190.

[37] S. Chen, X. Li and J. Iong. "Series arc fault identification for photovoltaic system based on time domain and time frequency domain analysis", in: IEEE journal of photovoltaics, 7.4 (2017).

[38] G. S. Seo, J. I. Ha, B. H. Cho "Series arc fault detection method based on statistical analysis for DC grids", in: IEEE Applied Power Electronics Conference and Exposition (APEC), (2016), pp. 487-492.

[39] G. S. Seo, K. A. Kim, K. C. Lee, K. J. Lee, B. H. Cho. "A new DC arc fault detection method using DC system component modeling in low frequency range", in: IEEE Applied Power Electronics Conference and Exposition (APEC), (2015), pp. 2438-2444.

[40] S. Chae, J. Park and S. Oh. "Series DC arc fault detection algorithm for DC microgrids using relative magnitude comparison", in: IEEE journal of emerging and selected topics in power electronics, 4.4 (2016).

[41] P. Schweitzer, C. Bonnet, R. Chu, E. Carvou, A. Ramzi. (2020). Series arcing faults voltage and current signatures in a DC low power network. [Data set]. Zenodo. http://doi.org/10.5281/zenodo.4298972

[42] A. Mokarian, A. Farahi, A. G. Delavar. "False positives reduction techniques in intrusion detection systems – A review", in: IJCNS International journal of computer science and network security, 13.10 (2013).

[43] S. Ruuska, W. Hämäläinen, S. Kajava, M. Mughal, P. Matilainen, J.Mononen. " Evaluation of the confusion matrix method in the validation of an automated system for measuring feeding behaviour of cattle", in: Behavioural Processes, 148 (2018), pp 56-62.

[44] T. Fawcett. "An introduction to ROC analysis", in: Pattern Recognition Letters, ROC Analysis in Pattern Recognition. 27.8 (2006), pp. 861–874.

[45] C.D. Brown, H. T. Davis. "Receiver operating characteristics curves and related decision measures: A tutorial", in: Chemometrics and Intelligent Laboratory Systems, 80.1 (2006), pp. 24–38.

[46] Visa, S. et al. "Confusion Matrix-based Feature Selection". In: MAICS (2011).